

Ab initio computation on the Fe *L*-edge X-ray emission spectroscopy of Fe-bearing MgSiO₃ perovskite

XIANLONG WANG* AND TAKU TSUCHIYA

Geodynamics Research Center, Ehime University, 2-5 Bunkyo-cho, Matsuyama 790-8577, Japan

ABSTRACT

We systematically investigated the *L*-edge X-ray emission spectroscopy (XES), a *3d*-to-*2p* transition, of Fe²⁺- and Fe³⁺-bearing MgSiO₃ perovskite under high pressure based on the internally consistent LSDA+*U* technique combined with the Slater-transition method. The Fe *L*-edge XES spectra can be used to directly interpolate the distribution of Fe-*3d* electrons including the spin states and coordination environments of iron. Our results show that the spin transition from the high-spin state to low-spin state of Fe²⁺ and Fe³⁺ can be identified easily by the *L*-edge XES technique. The valence state of Fe (2+ or 3+) can be verified by this, since a shift of the first main peak of Fe²⁺ across the spin transition of 2 eV, in good agreement with the experimental value (~1.6 eV), is significantly smaller than that of Fe³⁺ of 4 eV. The width of the *L*-edge XES of Fe³⁺ also depends strongly on the substitution sites (Mg or Si), meaning that its coordination environments might also be distinguishable based on the Fe *L*-edge XES spectra. These strong sensitivities to the Fe's states suggest that the high-resolution Fe *L*-edge XES would be a useful experimental technique to investigate Fe-bearing silicate minerals.

Keywords: First-principles method, *L*-edge XES, Fe-bearing MgSiO₃ perovskite, high pressures

INTRODUCTION

Iron is one of the dominant impurities in the minerals of the potential Earth's lower mantle (LM) such as in MgSiO₃ and MgO (e.g., Hemley and Cohen 1992; Irifune and Tsuchiya 2007). Therefore, behavior of Fe in different spin states, valence states, and coordination environments needs to be clarified to improve our understanding of the LM. Researchers have already focused extensively on the behavior of Fe in LM minerals, which can be affected by several factors such as pressure and concentration of dissolving trivalent aluminum (Al³⁺), which is believed to be another dominant impurity in LM minerals (Irifune 1997; Badro et al. 2003, 2004; Li et al. 2004, 2006; Frost and Langenhorst 2002; Nishio-Hamane et al. 2005; Lin et al. 2005; Catalli et al. 2010; Fujino et al. 2012). Frost and Langenhorst (2002) confirmed that a fraction of Fe³⁺, Fe³⁺/ΣFe, in Fe-bearing MgSiO₃ perovskite (Pv) increases with the concentration of increasing Al. The pressure-induced spin transition of Fe in Fe-bearing MgO (ferropericlase) and MgSiO₃ Pv and postperovskite (PPv) was observed via Fe *K*-edge X-ray emission spectroscopy (XES) or Mössbauer spectroscopy (Badro et al. 2003, 2004; Li et al. 2004, 2006; Lin et al. 2005; McCammon et al. 2008; Catalli et al. 2010; Fujino et al. 2012). However, interpretations of the results obtained by these techniques are sometimes ambiguous. For example, very similar spectral variations observed with increasing pressure were assigned to the spin transition of Fe from the initial high-spin (HS) to the final low-spin (LS) state (Li et al. 2004, 2006) or to the final intermediate-spin (IS) state (McCammon et al. 2008) in Mg-Pv. Furthermore, not only the stable spin states but also their site dependence continued to be

debated. Jackson et al. (2005) reported that in Fe³⁺-bearing Mg-Pv, iron at the Mg site (hereafter denoted A site) became LS in the LM pressure range. Nevertheless, some other experimental results showed that Fe³⁺ in the A site remains HS even up to 136 GPa (Li et al. 2006; Catalli et al. 2010). Recently, based on spectral measurements, Fujino et al. (2012) proposed that Fe³⁺ in the A site of Mg-Pv would move to the Si site (hereafter denoted B site) after 40 GPa and then would undergo a spin transition. Meanwhile, theoretical simulations were also conducted for better understanding of the spin transition behavior of Fe (Tsuchiya et al. 2006; Hsu et al. 2011; Fukui et al. 2012; Tsuchiya and Wang 2013), since the spin transition of Fe was suggested to impact physical properties of LM minerals such as density, sound velocity, thermal conductivity, and so on (Lin and Tsuchiya 2008; Catalli et al. 2010). Theoretical results also showed that the Fe spin transition strongly depends on its substitution sites and valence charges. Fe²⁺ incorporated into MgO and Fe³⁺ at the B site of Mg-Pv underwent the HS-LS transition in the LM pressure range, while no spin transition was observed when Fe was substituted at the A site of Mg-Pv with geophysically relevant Fe concentrations (Tsuchiya et al. 2006; Bengtson et al. 2009; Hsu et al. 2011, 2012; Metsue and Tsuchiya 2011, 2012; Fukui et al. 2012; Tsuchiya and Wang 2013). In those studies, no stability of the IS state was ensured, suggesting that there are still technical difficulties in high-pressure experiments to identify the valence state and coordination environment of Fe clearly. Indeed, the Fe *K*-edge XES technique often used in experiments (Badro et al. 2003, 2004; Li et al. 2004, 2006; Lin et al. 2005, 2008; McCammon et al. 2008; Catalli et al. 2010; Fujino et al. 2012) can only illustrate the spin state of Fe clearly, whereas it is not easy to distinguish between Fe²⁺ and Fe³⁺ and to identify the position, the A or B site, since the *K*-edge XES detects the

* E-mail: xianlong@sci.ehime-u.ac.jp

Fe $3p$ -orbital feature only.

Because the $2p$ -to- $3d$ transition is an electric-dipole transition that is allowed according to the selection rules, the Fe L -edge XES can directly describe the distribution and intensity of Fe- $3d$ characteristics and therefore can be used to illustrate features of valence orbitals of Fe in Fe-bearing LM minerals. Actually, one pioneering measurement on the Fe L -edge XES of ferropericline at high pressure was already done using the resonant XES technique (Lin et al. 2010). Their results showed that the pressure-induced spin crossover of ferrous Fe in MgO could be identified through the analysis of its L -edge XES, whose main peak was pushed up about 1.6 eV across the HS-LS transition. However, to the best of our knowledge, there are no experimental or theoretical reports about the Fe L -edge XES of Fe-bearing Mg-Pv, where the substitution mechanism of Fe is much more complicated than in MgO. In this study, we systematically investigated the Fe L -edge XES of Fe-bearing Mg-Pv under high pressure by using first-principles methods combined with the Slater-transition method to show the L -edge XES features of Fe in Fe-bearing Mg-Pv and to offer theoretical references for future experiments, where Fe in different spin states (HS or LS), valence states ($2+$ or $3+$), and substituted sites (A or B site) were considered.

COMPUTATIONAL DETAILS

The lattice structures of Fe-bearing Mg-Pv are obtained including the screened Coulomb interaction (U) for the Fe- $3d$ electrons based on the internally consistent LSDA+ U formalism (Cococcioni and de Gironcoli 2005; Tsuchiya et al. 2006; Metsue and Tsuchiya 2011; Tsuchiya and Wang 2013) implemented in the Quantum Espresso (QE) code (Giannozzi et al. 2009), where the planewave basis is used to describe valence orbitals and the effects of core electrons and nuclei are approximated by pseudo-potentials. All structure models presented in this work are simulated by taking a $2 \times 2 \times 1$ supercell of orthorhombic Mg-Pv containing 80 atoms with one substituted Fe ion, corresponding to an iron concentration of 0.0625. The planewave cutoff energy is 50 Ry and a $2 \times 2 \times 2$ Monkhorst-Pack grid is adopted for the supercell to sample the irreducible parts of the Brillouin zone (Monkhorst and Pack 1976). All these parameters are the same as those applied in our previous works for Fe $^{2+}$ and Fe $^{3+}$ -bearing Pv and PPv (Metsue and Tsuchiya 2011, 2012; Tsuchiya and Wang 2013). The two valence states of $2+$ and $3+$, two spin states of the HS and LS, and two substituted A and B sites of Fe are examined here. The IS state is also considered for some cases. To analyze one Fe $^{3+}$ ion at the A or B site clearly, one Al $^{3+}$ ion is simultaneously introduced at the B or A site, respectively, for charge neutrality. The position of Al $^{3+}$ is selected to minimize the Fe $^{3+}$ -Al $^{3+}$ distance, which is electrostatically more favorable than dissociated configurations of these trivalent cations (e.g., Tsuchiya and Wang 2013). In summary, a total of seven different spin and iron configurations are investigated in this study: (1) Fe $^{2+}$ doped at the A site in the HS (hereafter denoted as A $_{HS}^{2+}$); (2) in the LS (A $_{LS}^{2+}$), and (3) in the IS (A $_{IS}^{2+}$); (4) Fe $^{3+}$ substituted at the A site in the HS (A $_{HS}^{3+}$) and (5) in the LS (A $_{LS}^{3+}$); and (6) Fe $^{3+}$ doped at the B site in the HS (B $_{HS}^{3+}$) and (7) in the LS (B $_{LS}^{3+}$).

For each case, all the structural degrees of freedom, the cell parameters, and the atomic coordinates are fully relaxed

TABLE 1. On-site Coulomb interaction (U in eV) optimized for Fe in different valence states ($2+$ and $3+$), spin states (HS and LS state), and substitution sites (A and B site)

P (GPa)	A $_{HS}^{2+}$	A $_{LS}^{2+}$	A $_{HS}^{3+}$	A $_{LS}^{3+}$	B $_{HS}^{3+}$	B $_{LS}^{3+}$
0	6.74	5.05	3.93	5.32	3.64	5.11
30	4.44	5.14	3.91	5.30	3.60	5.25
60	3.85	5.23	3.89	5.33	3.59	5.35
120	3.64	5.40	3.89	5.45	3.62	5.50

at static pressures of 0, 30, 60, and 120 GPa with the U values non-empirically optimized for each iron configuration at each pressure by linear response procedures (Cococcioni and de Gironcoli 2005). The U values applied in this study are listed in Table 1, which are taken from our previous works about Fe $^{2+}$ -bearing (Metsue and Tsuchiya 2012) and Fe $^{3+}$ -bearing Mg-Pv (Tsuchiya and Wang 2013). Spectral features for the obtained structures are then calculated by using the CP2 K code (<http://www.cp2k.org>), which is based on the Gaussian and augmented planewave (GAPW) all-electron formalism (Lippert et al. 1999) combined with the Slater-transition potential method (Iannuzzi and Hutter 2007). These methods have been used in our previous works to calculate the X-ray spectra of nitrogen-doped graphene, and our simulated results agree well with experimental measurements (Wang et al. 2011, 2013). The Ahlrichs-pVDZ basis set is used for representing the atomic orbitals (Schäfer et al. 1992), while a cutoff of 280 Ry is adopted to expand the planewave. The spectra are convoluted by using the Gaussian function with a width of 0.3 eV (Iannuzzi and Hutter 2007). To illustrate effects of the Hubbard U correction clearly, the electronic structures and spectral features obtained in the framework of the generalized gradient approximation (GGA) (Perdew et al. 1996) are also calculated. Our test calculations show that the electronic structures presented in this paper obtained by using the CP2 K code agree well with the QE code counterparts.

ABOUT U VALUES

The LDA and GGA methods, mean-field type treatments, can describe systems with delocalized electrons well. However, they cannot accurately simulate the partially filled bands, where the electrons are strongly correlated and localized. Usually, representation for the large on-site Coulombic interaction among localized electrons can be improved by introducing the Hubbard U correction (e.g., Anisimov et al. 1991). To better extract the properties of Fe-bearing Mg-Pv, the Hubbard U correction is included in this work by means of an internally consistent method as mentioned in the previous section. The U values applied in the present calculations are presented in Table 1. Except for the case of A $_{HS}^{2+}$ at 0 GPa, the Hubbard U values are almost independent of pressure and Fe's valence state, and those for the LS state are generally 1.38–1.88 eV larger than the corresponding values of the HS state. As shown in Figure 3, this is partially because the distributions of the d orbitals in LS Fe $^{2+}$ and Fe $^{3+}$ are much more localized than the counterpart of HS Fe, which therefore acquires smaller U values due to weaker localization of the d electrons. In contrast, only at 0 GPa, A $_{HS}^{2+}$ acquires a U value of 6.74 eV, which is anomalously larger than that of A $_{LS}^{2+}$ (5.05 eV). This is likely related to the pressure that is out of the stability range of Mg-Pv.

A similar theoretical work about the U values in Fe- and Al-bearing Mg-Pv were done via the same method Hsu et al.

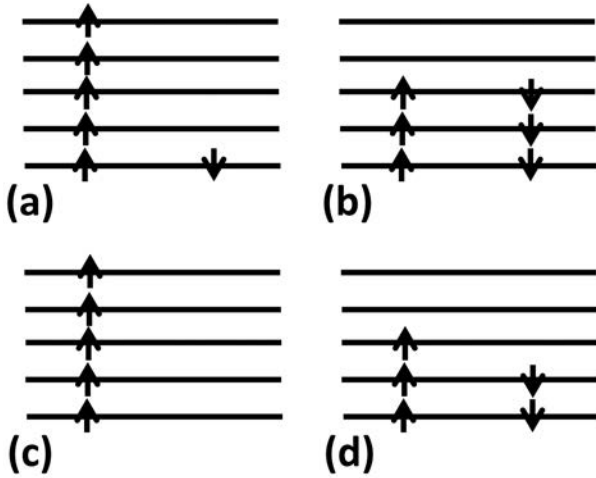


FIGURE 1. Schematic diagrams of the distributions of Fe 3d electrons. (a and b, respectively) show the Fe²⁺ cases in the high-spin and low-spin state, and (c and d) the corresponding parts of the Fe³⁺ cases. Up (down) arrows represent the electron with spin up (down), respectively.

(2012) used and their U values showed some discrepancies with our values (± 0.25 eV at most). They, however, determined the U values for systems with an Fe concentration of 12.5%, whereas we examined a smaller and more reasonable Fe concentration of 6.25% in this work. The major reason for the small differences in U in two works could possibly be attributed to the fact that the U value could change depending on the Fe concentrations. Although there are some discrepancies in U , those were found to produce insignificant effects on the XES spectra as shown below.

RESULTS AND DISCUSSION

Before discussing the calculated electronic structures in detail, we first present the distribution of the 3d electrons of Fe²⁺ and Fe³⁺ in the HS and LS to understand the simulated results more clearly (Fig. 1) based on the traditional crystal field theory (Burns 1993). Since the valence electron configuration of neutral Fe⁰ is 3d⁶4s², the HS state of Fe²⁺ (3d⁶) has a magnetic moment of 4 μ_B , indicating that five d electrons occupy the spin-up state while the remaining occupy the spin-down state (Fig. 1a). For the case of LS Fe²⁺, half (three) of the d electrons occupy the spin-up and -down state equally, leading to a total magnetic moment of zero (Fig. 1b). As shown in Figures 1c and 1d, the HS and LS states of Fe³⁺, respectively acquire the magnetic moments of 5 and 1 μ_B , since Fe³⁺ possesses only five d electrons.

As the partial density of states (pDoS) of the Fe-3d orbital in A_{HS}²⁺ under pressures of 30 and 120 GPa (see Fig. 2), the electronic structure of Fe in Fe-bearing Mg-Pv is insensitive to pressure, and only the width of occupied bands slightly increases with increasing pressure due to a decrease in the distances between Fe and its neighboring oxygen. Since the pressure-induced spin transitions of Fe in Fe-bearing Mg-Pv are usually observed in the range of 40~100 GPa (e.g., Badro et al. 2004), the calculated pDoS of the Fe 3d orbital in the HS (LS) state at 30 (120) GPa corresponds to pressures before (after) the spin transition and are respectively shown in Figure 3. The simulated distributions

of Fe 3d electrons are consistent with the schematic diagrams shown in Figure 1, such as that A_{HS}²⁺ and A_{LS}²⁺ have a total magnetic moment of 4.0 and 0.0 μ_B , respectively. The electronic structures obtained within the GGA are distinctly different from that of the LSDA+ U . For example, systems containing A_{HS}²⁺ and B_{LS}³⁺ become metallic based on the GGA, while the LSDA+ U clearly show that they have insulating ground states, respectively, with 1.18 and 1.44 eV band gaps. For some other cases, the GGA was found to produce insulating ground states but with band gaps that were too small. The LSDA+ U can mend this notably. Experimental observation showed that at 23 GPa and depending on temperature, (Mg_{0.93}Fe_{0.07})SiO₃ Pv has an insulating band gap from 0.41 to 0.92 eV (Katsura et al. 1998). For each case, the 3d occupation depends strongly on the spin states of Fe, and it becomes much more localized after the HS to LS state transition, partially because the orbital splitting caused by the crystal field does not affect the distribution of LS occupied states. For example, when Fe substitutes at the B site and acquires the splitting between t_{2g} and e_g orbitals induced by the octahedral crystal field, both t_{2g} and e_g states of the spin-up branch are occupied in the HS configuration, while Fe-3d electrons only distribute along the t_{2g} orbital

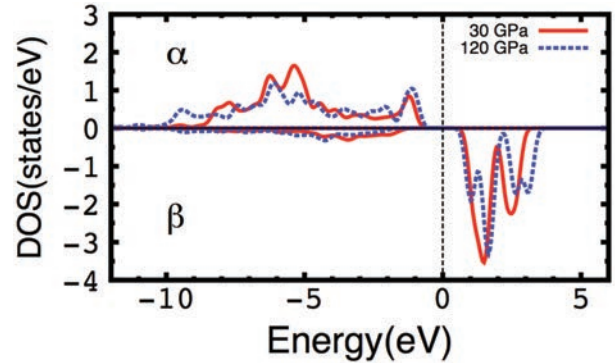


FIGURE 2. Fe 3d partial density of states (pDoS) for A_{HS}²⁺ under pressures of 30 and 120 GPa are shown in red-solid and blue-dashed line, respectively. (α and β , respectively) denote the spin-up and -down states. The vertical dashed line located at 0 eV represents the Fermi level. (Color online.)

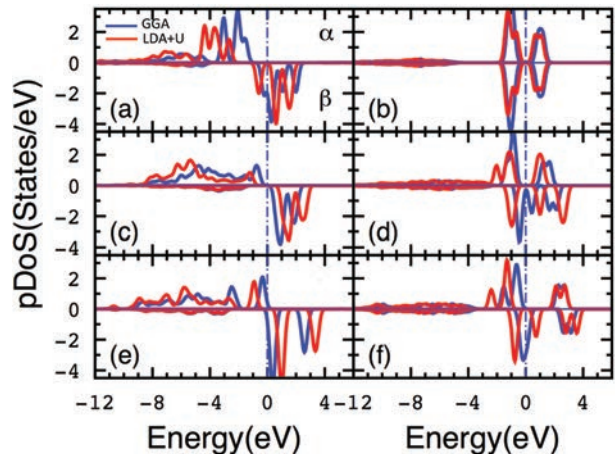


FIGURE 3. Fe 3d pDoS for A_{HS}²⁺ (a), A_{LS}²⁺ (b), A_{HS}³⁺ (c), A_{LS}³⁺ (d), B_{HS}³⁺ (e), and B_{LS}³⁺ (f). (Color online.)

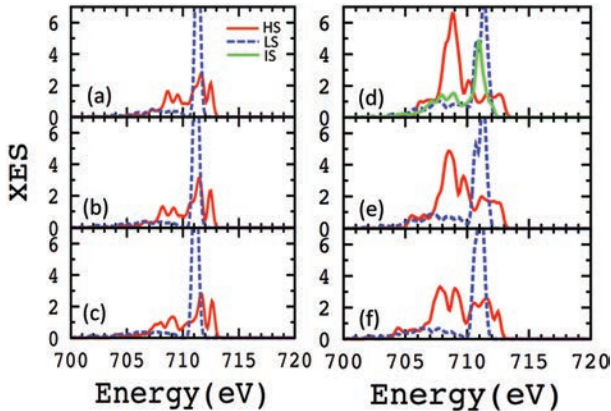


FIGURE 4. Calculated Fe *L*-edge XES spectra of $A_{\text{HS,LS}}^{2+}$ -bearing Mg-Pv. The GGA results at 30, 60, and 120 GPa are shown in **a**, **b**, and **c**, while the counterparts from the LSDA+*U* are in **d**, **e**, and **f**, respectively. To clearly illustrate the spectral features of HS Fe based on the LSDA+*U* method, its intensity is magnified two times. (Color online.)

in the LS cases as already mentioned schematically in Figure 1.

The simulated XES of A^{2+} , A^{3+} , and B^{3+} are, respectively, presented in Figures 4, 5, and 6. Similar to the pDoS, the *L*-edge XES of Fe also depends weakly on pressure, so that only the spectra under 30, 60, and 120 GPa, corresponding to pressures before, undergoing, and after the HS-LS transition, respectively, are shown. The spectra simulated within the GGA are also presented to help illustrate the effects of *U* correction. Within the LSDA+*U*, one main peak located at 709.0 eV is observed for the A_{HS}^{2+} case at 30 GPa, while one localized main peak appears at 711.0 eV for the A_{LS}^{2+} case at 120 GPa, indicating that the main peak of *L*-edge XES of Fe^{2+} substituted in the A site would be pushed up by ~ 2 eV across the HS-LS transition. The sharpness of the main peaks of the LS Fe reflects the higher localization of the *3d* electron in the LS state as shown in Figure 3. Although the intensity of the main peak of A_{HS}^{2+} decreases with increasing pressure, the shift of the main peak and the change in its sharp-

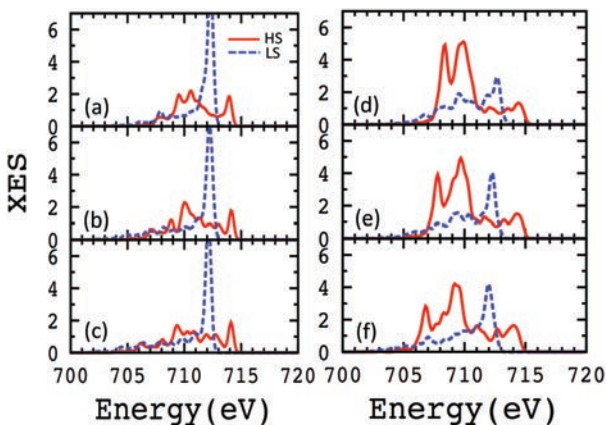


FIGURE 5. Calculated Fe *L*-edge XES spectra of $A_{\text{HS,LS}}^{3+}$ -bearing Mg-Pv. The GGA results at 30, 60, and 120 GPa are shown in **a**, **b**, and **c**, while the LSDA+*U* counterparts are in **d**, **e**, and **f**, respectively. (Color online.)

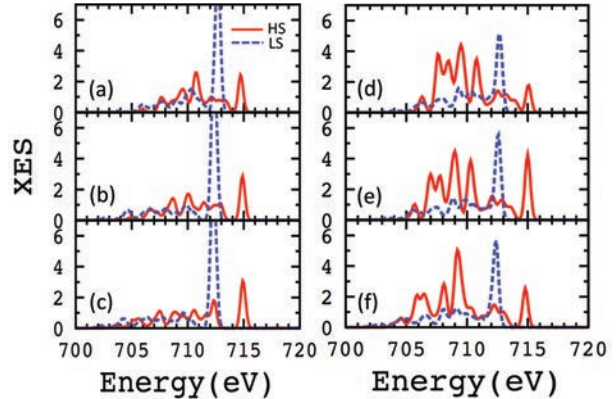


FIGURE 6. Calculated Fe *L*-edge XES spectra of $B_{\text{HS,LS}}^{3+}$ -bearing Mg-Pv. The GGA results at 30, 60, and 120 GPa are shown in **a**, **b**, and **c**, while the counterparts from the LSDA+*U* are in **d**, **e**, and **f**, respectively. (Color online.)

ness can therefore be available to identify the spin state of Fe^{2+} in Mg-Pv. In contrast, the spectral features from the GGA do not show any difference in the main peak position between the HS and LS cases except for some small localization. Our results based on the LSDA+*U* agree well with experimental observations (Lin et al. 2010), where a shift up (~ 1.6 eV) of the main peak of the Fe *L*-edge XES of ferropervicite was clearly observed during the spin transition. This again demonstrates that the Hubbard *U* correction is a key to describing the XES features of Fe-bearing minerals properly. For IS Fe^{2+} at the A site, acquiring a magnetic moment of $1 \mu_B$, its stabilization in Mg-Pv is still under discussion. It was experimentally suggested to be a stable configuration (McCammon et al. 2008). However, previous theoretical works proposed a contrary opinion, since it has an enthalpy as much as 0.5 eV/Fe higher than the most stable case, HS Fe^{2+} at the A site, for the whole LM pressure range (Bengtson et al. 2008; Hsu et al. 2010). The Fe *L*-edge XES technique should be a potential indicator about whether IS Fe^{2+} at the A site will appear or not and can provide useful information for experimental analysis. Therefore, the *L*-edge XES spectra of IS Fe^{2+} in the A site of Pv at 30 GPa were simulated as a test to show the general features of IS Fe^{2+} at the A site, where the *U* value of 5.03 eV, obtained through the linear response method, was applied. As shown in Figure 4d, one main peak located at ~ 711 eV, which is very close to that of LS Fe^{2+} , is observed in the calculated XES of IS Fe^{2+} . Since the major spectral features of IS Fe^{2+} are very similar to LS Fe^{2+} , it is difficult to distinguish IS Fe^{2+} from LS Fe^{2+} by using the Fe *L*-edge XES technique. Note that although using very similar methods, the *U* values could be slightly different depending on the discrepancies of the calculation conditions, (e.g., iron concentration, as we mentioned previously). (Hsu et al. 2012; Tsuchiya and Wang 2013) To clarify how the uncertainty in *U* affects the XES features, we examined the spectra of all iron configurations at 30 GPa with variations of the *U* value. *U* value ± 1 eV, which is sufficiently larger than the typical numerical uncertainty in *U*, were applied. For both HS and LS Fe, their major spectral features (e.g., the main peak positions) were found to still remain unchanged, while it only changed the relative intensities of the main peaks a little.

As shown in Figures 5 and 6, the spectral features of Fe³⁺ obtained via GGA are also significantly different from those obtained via LSDA+*U*. We hereafter focus only on the LSDA+*U* results. Unlike the cases of A_{HS}²⁺, where only one sharp main peak appears, two and four main peaks are, respectively, observed in the range of 1.8 and 3.5 eV for the A_{HS}³⁺ and B_{HS}³⁺ cases at 30 GPa. This can be explained by the relatively broader distribution of the occupied states of Fe³⁺ 3*d* compared to that of Fe²⁺ (see Fig. 3), since the 3*d* levels for Fe³⁺ are deeper due to a stronger attractive potential, which leads to a stronger hybridization with the O 2*p* valence band. Differences between spectra of Fe²⁺ and Fe³⁺ were therefore attributed mainly to their different attractive potentials. These clear differences in the main peaks suggest that their profile and position could be a good indicator to distinguish between A_{HS}²⁺, A_{HS}³⁺, and B_{HS}³⁺. They are pushed up and converged to one main peak located about 712.0 eV after the spin transition, indicating that similarly to the case of Fe²⁺, the spin transition of Fe³⁺ can also be identified by the shift and the change in sharpness of their main peaks. These spectral transmutations across the spin transition basically reflect the differences in the ground states electronic structures as shown in Figure 3. As we mentioned above, the distribution of the occupied states of LS Fe 3*d* is much narrower than HS Fe, since the orbital splitting caused by the crystal field is included only in the occupied states of HS Fe 3*d*. In contrast, the splitting can be observed above the occupied states in LS Fe 3*d*, which is not detected by *L*-edge XES. The shift of the first main peaks of Fe³⁺ (4 eV) is, however, about two times larger than that of Fe²⁺ (2 eV). Therefore, the valence state (2+ or 3+) of Fe would also be clearly distinguishable by detecting the shift of the first main peaks in the Fe *L*-edge XES across the spin transition. As shown in Figures 5d and 6d, the widths not only of the main peaks but also of the whole spectra for the A_{HS}³⁺ case (7.0 eV) are notably narrower than the counterparts for the B_{HS}³⁺ case (9.0 eV). This is because the average distance between oxygen and Fe of 1.87 Å in the B_{HS}³⁺ case is substantially shorter than the counterpart (2.03 Å) in the A_{HS}³⁺ case, and thus the hybridization between iron and oxygen is larger in the B site than in the A site. These results suggest that the width of the main peaks or whole spectra could be used to identify the coordination environment of Fe³⁺ (the Mg or Si site). These discussions strongly suggest that all of the spin states, valence states, and substitution sites of Fe in Mg-Pv are potentially distinguishable by analyzing the features of the Fe *L*-edge XES. In summary, the spin state could be clearly identified by the shift and sharpness of the main peaks across the spin transition, the valence state can be identified by the profile of the main peaks in the HS state and also by the shift of the first main peak across the spin transition, and the substituted site could be identified also by the forms of both main peaks and whole spectra. Finally, we would like to mention the limitations of our present simulation. The multiplet effects describing the coupling between the 2*p* and 3*d* orbitals, which can introduce some minor spectral features such as the satellite peak (*Kβ'*) of the Fe *K*-edge XES (Badro et al. 2004), are not included in this work, since the simple Slater-transition method is applied. However, we believe that our results can describe the spectral features of Fe-bearing Mg-Pv under high pressure sufficiently, mainly because high-pressure Fe *L*-edge spectral experiments can usually detect only

the major spectral features due to non-hydrostaticity, limited amount of sample, etc. (Lin et al. 2010). This is also the reason why all the discussion in this work focused on the main features of the simulated spectra. Since the 2*p* hole spin-orbit coupling was also not considered in present calculations, the simulated spectra do not show the splitting between the *L*₂ and *L*₃ peak. Our simulated results can present the features of a dominant *L*₃ peak, which is the main target of mineral spectral analysis (Van Aken et al. 1998; Lauterbach et al. 2000; Lin et al. 2010). Both *L*₂ and *L*₃ peaks show similar features, but the magnitude of the *L*₂ peak is lower than *L*₃.

IMPLICATIONS

The *L*-edge XES features of Fe in Fe-bearing MgSiO₃ Pv were investigated by the all-electron density functional method for the first time, combined with the internally consistent LSDA+*U* and the Slater-transition potential techniques. Different spin states (high- and low-spin), valence states (2+ and 3+), and substitution sites (Mg and Si site) of Fe were examined. Our results showed that both the spin states and the valence states of Fe can clearly be illustrated by a shift of the first main peaks across the spin transition. Furthermore, the widths of the main peaks and the whole spectra of Fe in the high-spin state were found to be available to distinguish the substituted sites. Based on these theoretical predictions we propose that the Fe *L*-edge XES measurement is a useful experimental technique to study the state of iron in Fe-bearing lower mantle minerals. We invite corresponding experiments.

ACKNOWLEDGMENTS

We thank S. Whitaker for comments. This research was supported by JSPS Grants-in-Aid for Scientific Research under Grant No. 25 03023, KAKENHI 20001005 and 21740379, and the Ehime University Global COE program “Deep Earth Mineralogy.”

REFERENCES CITED

- Anisimov, V.I., Zaanen, J., and Andersen, O.K. (1991) Band theory and Mott insulators: Hubbard *U* instead of Sonner I. *Physical Review B*, 44, 943–954.
- Badro, J., Fiquet, G., Guyot, F., Rueff, J.P., Struzhkin, V.V., Vankó, G., and Monaco, G. (2003) Iron partitioning in Earth’s mantle: Toward a deep lower mantle discontinuity. *Science*, 300, 789–791.
- Badro, J., Rueff, J.P., Vankó, G., Monaco, G., Fiquet, G., and Guyot, F. (2004) Electronic transitions in perovskite: Possible nonconvecting layers in the lower mantle. *Science*, 305, 383–386.
- Bengtson, A., Persson, K., and Morgan, D. (2008) *Ab initio* study of the composition dependence of the pressure induced spin crossover in perovskite (Mg_{1-x}Fe_x)SiO₃. *Earth and Planetary Science Letters*, 265, 535–545.
- Bengtson, A., Li, J., and Morgan, D. (2009) Mössbauer modelling to interpret the spin state of iron in (Mg,Fe)SiO₃ perovskite. *Geophysical Research Letters*, 36, L15301.
- Burns, R.G. (1993), *Mineralogical Applications of Crystal Field Theory*. Cambridge University Press, U.K.
- Catalli, K., Shim, S.H., Prakapenka, V.B., Zhao, J., Sturhahn, W., Chow, P., Xiao, Y., Liu, H., Cynn, H., and Evans, W.J. (2010) Spin state of ferric iron MgSiO₃ perovskite and its effect on elastic properties. *Earth and Planetary Science Letters*, 289, 68–75.
- Cococcioni, M., and de Gironcoli, S. (2005) Linear response approach to the calculation of the effective interaction parameters in the LSDA+*U* method. *Physical Review B*, 71, 035105.
- Frost, D.J., and Langenhorst, F. (2002) The effect of Al₂O₃ on Fe-Mg partitioning between magnesio-wüstite and magnesium silicate perovskite. *Earth and Planetary Science Letters*, 199, 227–241.
- Fujino, K., Nishio-Hamane, D., Seto, Y., Sata, N., Nagai, T., Shinmei, T., Irifune, T., Ishii, H., Hiraoka, N., Cai, Y., and Tsuei, K.D. (2012) Spin transition of ferric iron in Al-bearing Mg-perovskite up to 200 GPa and its application for the lower mantle. *Earth and Planetary Science Letters*, 317-318, 407–412.
- Fukui, H., Tsuchiya, T., and Baron, A.Q.R. (2012) Lattice dynamics calculations for ferropericlaise with internally consistent LSDA+*U* method. *Journal of*

- Geophysical Research, 117, B12202.
- Giannozzi, P., Baroni, S., Bonini, N., Calandra, M., Car, R., Cavazzoni, C., Ceresoli, D., Chiarotti, G.L., Cococcioni, M., Dabo, I., and others. (2009) QUANTUM ESPRESSO: A modular and open-source software project for quantum simulations of materials. *Journal of Physics: Condensed Matter*, 21, 395502.
- Hemley, R.J., and Cohen, R.E. (1992) Silicate perovskite. *Annual Review of Earth and Planetary Sciences*, 20, 553–600.
- Hsu, H., Umemoto, K., Blaha, P., and Wentzcovitch, R.M. (2010) Spin states and hyperfine interactions of iron in (Mg,Fe)SiO₃ perovskite under pressure. *Earth and Planetary Science Letters*, 294, 19–26.
- Hsu, H., Blaha, P., Cococcioni, M., and Wentzcovitch, R.M. (2011) Spin-state crossover and hyperfine interactions of ferric iron in MgSiO₃ perovskite. *Physical Review Letters*, 106, 118501.
- Hsu, H., Yu, Y.G., and Wentzcovitch, R.M. (2012) Spin crossover of iron in aluminous MgSiO₃ perovskite and post-perovskite. *Earth and Planetary Science Letters*, 359, 34–39.
- Iannuzzi, M., and Hutter, J. (2007) Inner-shell spectroscopy by the Gaussian and augmented planewave method. *Physical Chemistry Chemical Physics*, 9, 1599–1610.
- Irifune, T. (1997) Absence of an aluminous phase in the upper part of the Earth's lower mantle. *Nature*, 370, 131–133.
- Irifune, T., and Tsuchiya, T. (2007) Mineralogy of the Earth—Phase transitions and mineralogy of the lower mantle. In G.D. Price, Ed., *Mineral Physics*, 2, p. 33–62. *Treatise on Geophysics*, Elsevier, Amsterdam.
- Jackson, J.M., Struhahn, W., Shen, G., Zhao, J., Hu, M.Y., Errandonea, D., Bass, J.D., and Fei, Y. (2005) A synchrotron Mössbauer spectroscopy study of (Mg,Fe)SiO₃ perovskite up to 120 GPa. *American Mineralogist*, 90, 199–205.
- Katsura, T., Sato, K., and Ito, E. (1998) Electrical conductivity of silicate perovskite at lower-mantle conditions. *Nature*, 395, 493–495.
- Lauterbach, S., McCammon, C.A., van Aken, P., Langenhorst, F., and Seifert, F. (2000) Mössbauer and ELNES spectroscopy of (Mg,Fe)(Si,Al)O₃ perovskite: A highly oxidised component of the lower mantle. *Contributions to Mineralogy and Petrology*, 138, 17–26.
- Li, J., Struzhkin, V.V., Mao, H.K., Shu, J., Hemley, R.J., Fei, Y., Mysen, B., Dera, P., Prakapenka, V., and Shen, G. (2004) Electronic spin state of iron in lower mantle perovskite. *Proceedings of the National Academy of Sciences*, 101, 14027–14030.
- Li, J., Struhahn, W., Jackson, J.M., Struzhkin, V.V., Lin, J.F., Zhao, J., Mao, H.K., and Shen, G. (2006) Pressure effect on the electronic structure of iron in (Mg,Fe)(Al,Si)O₃ perovskite: A combined synchrotron Mössbauer and X-ray emission spectroscopy study up to 100 GPa. *Physics and Chemistry of Minerals*, 33, 575–585.
- Lin, J.F., and Tsuchiya, T. (2008) Spin transition of iron in the Earth's lower mantle. *Physics of the Earth and Planetary Interiors*, 170, 248–259.
- Lin, J.F., Struzhkin, V.V., Jacobsen, S.D., Hu, M., Chow, P., Kung, J., Liu, H., Mao, H.K., and Hemley, R.J. (2005) Spin transition of iron in magnesiowüstite in Earth's lower mantle. *Nature*, 436, 377–380.
- Lin, J.F., Mao, Z., Jarrige, I., Xiao, Y., Chow, P., Okuchi, T., Hiraoka, N., and Jacobsen, S.D. (2010) Resonant X-ray emission study of the lower-mantle ferropericlase at high pressures. *American Mineralogist*, 95, 1125–1131.
- Lippert, G., Hutter, J., and Parrinello, M. (1999) The Gaussian and augmented-plane-wave density functional method for ab initial molecular dynamics simulations. *Theoretical Chemistry Accounts*, 103, 124–140.
- McCammon, C., Kantor, I., Narygina, O., Rouquette, J., Ponkratz, U., Sergueev, I., Mezouar, M., Prakapenka, V., and Dubrovinsky, L. (2008) Stable intermediate-spin ferrous iron in lower-mantle perovskite. *Nature Geoscience*, 1, 684–687.
- Metsue, A., and Tsuchiya, T. (2011) Lattice dynamics and thermodynamic properties of (Mg,Fe²⁺)SiO₃ postperovskite. *Journal of Geophysical Research*, 116, B08207.
- (2012) Thermodynamic properties of (Mg,Fe²⁺)SiO₃ perovskite at lower mantle pressures and temperatures: An internally consistent LSDA+U study. *Geophysical Journal International*, 190, 310–322.
- Monkhorst, H.J., and Pack, J.D. (1976) Special points for Brillouin-zone integrations. *Physical Review B*, 13, 5188–5192.
- Nishio-Hamane, D., Nagai, T., Fujino, K., Seto, Y., and Takafuji, N. (2005) Fe³⁺ and Al solubilities in MgSiO₃ perovskite: Implication of the Fe³⁺AlO₃ substitution in MgSiO₃ perovskite at the lower mantle condition. *Geophysical Research Letters*, 32, L16306.
- Perdew, J.P., Burke, K., and Ernzerhof, M. (1996) Generalized gradient approximation made simple. *Physical Review Letters*, 77, 3865–3868.
- Schäfer, A., Horn, H., and Ahlrichs, R. (1992) Fully optimized contracted Gaussian basis sets for atoms Li to Kr. *Journal of Chemical Physics*, 97, 2571–2577.
- Tsuchiya, T., and Wang, X. (2013) Ab initial investigation on the high-temperature thermodynamic properties of Fe³⁺-bearing MgSiO₃ perovskite. *Journal of Geophysical Research*, 118, 1–9.
- Tsuchiya, T., Wentzcovitch, R.M., da Silva, C.R.S., and de Gironcoli, S. (2006) Spin transition in magnesiowüstite in Earth's lower mantle. *Physical Review Letters*, 96, 198501.
- Van Aken, P.A., Liebscher, B., and Styrsa, V.J. (1998) Quantitative determination of iron oxidation states in minerals using Fe L_{2,3}-edge electron energy-loss near-edge structure spectroscopy. *Physics and Chemistry of Minerals*, 25, 323–327.
- Wang, X.L., Hou, Z.F., Ikeda, T., Huang, S.F., Terakura, K., Boero, M., Oshima, M., Kakimoto, M., and Miyata, S. (2011) Selective nitrogen doping in graphene: Enhanced catalytic activity for the oxygen reduction reaction. *Physical Review B*, 84, 245434.
- Wang, X.L., Hou, Z.F., Ikeda, T., Oshima, M., Kakimoto, M., and Terakura, K. (2013) Theoretical characterization of X-ray absorption, emission, and photoelectron spectra of nitrogen doped along graphene edges. *Journal of Physical Chemistry A*, 117, 579–589.

MANUSCRIPT RECEIVED FEBRUARY 26, 2013

MANUSCRIPT ACCEPTED SEPTEMBER 11, 2013

MANUSCRIPT HANDLED BY RENATA WENTZCOVITCH